Subsurface Domain Image Warping by Horizontal Contraction and its Application to Wave-Equation Migration Velocity Analysis

Peng Shen, Shell International E&P, William W. Symes, Rice University

SUMMARY

A kinematically correct choice of velocity focuses subsurface offset image gathers at zero offset. Infinitesimal warping from the current image towards its focus can be approximated by a horizontal contraction. The image residual can be then taken as the difference between the warped and the original image to account for the velocity error. Least squares fitting of the effect of a velocity perturbation to this image warping perturbation produces a tomographic velocity update. This paper describes the warping scheme based on the radial image derivative in subsurface offset. We show the corresponding gradient is free of the diffraction edge effect. We further enhance the efficiency of the velocity update procedure via use of a diagonal Hessian approximation.

INTRODUCTION

For classical full waveform inversion, the observed data is naturally treated as a reference. The difference between the synthetic and the observed data (data residual) drives velocity updating through minimization of its mean square (Tarantola and Vallette, 1982; Pratt et al., 1998). Wave-equation reflection tomography is often posed in the image domain, where there is no natural reference image that can be used for comparison. Sava (2000) proposed a method to obtain a reference image via Stolt residual migration based on the information generated in the current migration. Differential semblance (DS) reflection tomography defines the residual by scaling the image by offset (Shen and Symes, 2008). Fei and Williamson (2010) reported a DS type image residual using an infinitesimal offset contraction, while Albertin (2011) explicitly used two infinitesimally separated images to produce image residual aided with a local re- and de-migration using one-way propagators. It is not clear how to extend Albertin's algorithm into general propagators.

Waveform tomography maps the image residual to a search direction in velocity model space. For DS and similar algorithms, the search direction is (or is closely related to) the gradient of an objective function. The various choices of residual definition are not equivalent: in particular, reflector truncations and other singularities lead to oscillations in DS gradient (so-called gradient artifacts) which lead in turn to slow convergence and to the need for significant update smoothing. Image residuals obtained as differences between infinitesimally separated images appear to lead to velocity updates which avoid these artifacts. These updates are on the other hand not gradients of objective functions.

All waveform-tomographic updates, including DS, may be viewed as least-squares projections of image updates into velocity model space. The rule for forming image updates may be viewed as a vector field (differential equation) on image space, limit points of which are focused (physical) images. Velocity estimation amounts to solving the projected differential equation in model space by a marching method.

This paper describes a warping method, based on the radial offset derivative, that generates infinitesimally improved images from current images. We demonstrate that the velocity update from the corresponding image residual is artifact-free. We note that this velocity update is not the gradient of an objective function. The key to efficiency is fast computation of the projection into model space; we introduce an approximate Hessian inverse which renders this projection practical at industry scale.
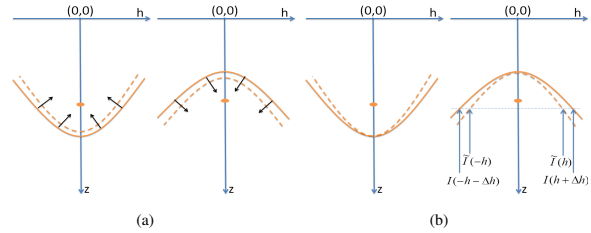
METHOD

Figure 1: Schematic illustration of image in subsurface offset. (a) Events obtained with a faster or slower velocity curve up(left) or down(right), respectively. Black arrows indicate warping direction. The solid and the dashed curve represent the current and the infinitesimally warped image, respectively. (b)Total warping approximated by the horizontal contraction.

A 2D subsurface offset image gather for layered reflections (horizontal or tilted - makes no difference) shows a shape similar to that depicted in Fig.1(a). Depending on whether the migration velocity pertaining to the event is greater or smaller than the true velocity, the image in subsurface offset curves upward or downward, respectively. In both cases, the events have a curvature direction along which a infinitesimal shift from the original image makes the final image slightly more focused. The image corresponding to the correct velocity is always on the $h = 0$ axis, near the envelope of the normal line to the initial image. Motion or warping by inward curvature is difficult to implement. However, a good approximation can be obtained by ignoring the vertical shift. As shown in Fig.1(b), a horizontal contraction represented by the dashed curves well approximates the inward warping except points at zero offset. Let $\tilde{I}$ denote the infinitesimally warped image from the current image I by a small amount Δh. Let x be the image point and h be the horizontal subsurface offset: then for $h \in R$

$$
\begin{aligned}
\tilde{I}(x,h) &= I(x,h+\Delta h) & h > 0 \\
\tilde{I}(x,h) &= I(x,h-\Delta h) & h < 0.
\end{aligned}
\tag{1}
$$

We regard $\tilde{I}$ as an infinitesimally improved image, moved slightly

towards the true (focused) image. The difference between $\tilde{I}$ and I can be expressed via the radial derivative $\partial_{|h|}$

$$\delta I = \tilde{I} - I \simeq \partial_{|h|} I \Delta h \qquad (2)$$

where

$$\partial_{|h|} = \hat{h} \cdot \nabla_h, \qquad (3)$$

$\hat{h}$ is the unit horizontal subsurface offset vector, $|h|$ is the radius or length of the vector h, ∇_h is the gradient operator in h, and Δh is a uniform increment of horizontal offset along the radial direction. Equations (2) and (3) are also correct as written in 3D (for 2D offset vector h).

While the warping formula (2) drives the image towards focus, it is not the result of migrating the same data with a different velocity. Therefore, we project the image difference expressed in equation (2) into velocity space by solving the equation

$$\left(\frac{\partial I}{\partial c} \right) \delta c = \delta I \qquad (4)$$

for a velocity update δc. Since equation (4) is very unlikely to have a literal solution, we solve it in the least squares sense, that is,

$$\delta c = H^{-1} g, \qquad (5)$$

in which

$$H = \left(\frac{\partial I}{\partial c} \right)^* K \left(\frac{\partial I}{\partial c} \right)$$

is the Hessian of the least squares objective

$$J[\delta c] = \frac{1}{2} \left\| L \left(\left(\frac{\partial I}{\partial c} \right) \delta c - \delta I \right) \right\|^2,$$

and

$$g = \left(\frac{\partial I}{\partial c} \right)^* K \delta I \qquad (6)$$

is its gradient. $K = L^* L$ and L is a suitable preconditioning operator in image space.

The rule (5) produces a velocity update for any choice of image residual δI. For example, Fei and Williamson (2010) suggested

$$\delta I_{FW} = h \cdot \nabla_h I. \qquad (7)$$

which differs from δI specified in equation (2) by an additional factor of $|h|$. Alternatively, "classical" differential semblance, as for example in (Shen and Symes, 2008), uses

$$\delta I_{DS} = A^* A I, \qquad (8)$$

in which A is any operator on image space which vanishes on focused images - multiplication by $|h|$ is the conventional choice. The residual defined in equation (8) is the image gradient of the objective function $J = \frac{1}{2} \|AI\|_{L_2}^2$. Neither δI given by equation (2) nor δI_{FW} given by equation (7) is the gradient of an objective function, and indeed the operators involved in these latter two residual formulae are non-symmetric.

For industry scale problems, iterative schemes for inverting the Hessian H often become prohibitively expensive. Fei and

Williamson (2010) use the approximation $H = $ identity operator. An economic and much more accurate approximation to equation (5) stems from the observation that

$$\widetilde{H_d} = \left(\frac{\partial I}{\partial c} \right)^* K \left(\frac{\partial I}{\partial c} \right) 1_c$$

approximates the diagonal of the Hessian, where 1_c is a constant velocity perturbation field that has unit value everywhere. Jointly influenced by the data and the current velocity, the diagonal of the Hessian H_d has a physical meaning of ray coverage. We then write the approximate solution to equation (4) as

$$\widetilde{\delta c}(x) = -\Delta h \frac{g(x)}{\widetilde{H_d}(x)} \qquad (9)$$

in which the inverse Hessian is replaced by a pointwise division of the gradient g by the approximate diagonal of the Hessian at every x. All operations are straightforward wave-equation computations as described in Shen (2012).

2D SYNTHETIC EXAMPLES
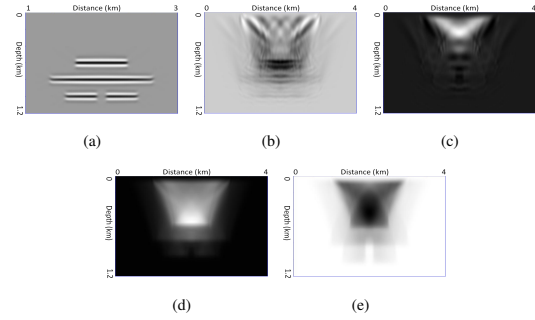

(a) (b) (c)

(d) (e)

Figure 2: (a) Image with correct velocity. (b)-(e) are gradients obtained according to equation (6) at different velocities and with different image residuals: (b) Slower velocity, $R = h^2 I$. (c) Faster velocity, $R = h^2 I$. (d) Slower velocity, $R = -\partial_{|h|} I$. (e) Faster velocity, $R = -\partial_{|h|} I$.

We first demonstrate by examples that the image residual induced by horizontal infinitesimal contraction does not produce gradient artifacts. Figure (2(a)) shows the image of reflectors designed to have clear edges. Using conventional DS image residuals, such as $\delta I = h^2 I$, we obtain gradient according to equation (6) (with K set equal to the identity operator) as shown in fig.2(b) and fig.2(c) for slower and faster velocities, respectively. The white color is negative and black is positive. Compared with one-way propagators, the reverse-time propagation kernel actually produces stronger and more complicated diffraction edge effects in gradients. Shown in fig.2(d) and fig.2(e) are gradients obtained with slower and faster velocities, respectively, using image residuals $\delta I = -\partial_{|h|} I$. Clearly, with the same gradient operator $\left(\frac{\partial I}{\partial c} \right)^*$, the image residual induced by radial derivative produces gradients not only correct in sign but also free of oscillatory artifacts.

We further test the Gauss-Newton scheme for velocity update using equation (9). Again, we use the word "gradient" to re-
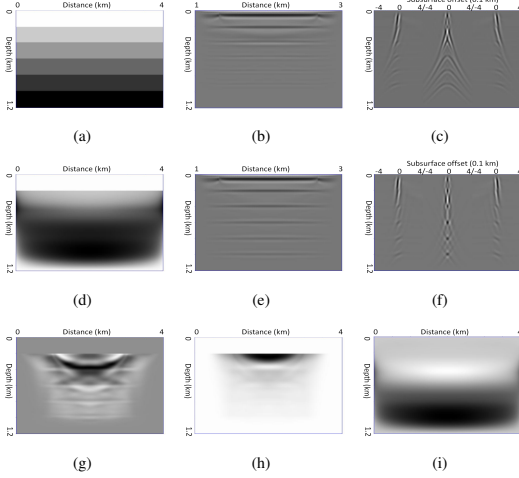
Figure 3: (a) Correct velocity. (b) Initial image. (c) Initial offset gather. (d) Velocity at iter. 20. (e) Image at iter. 20. (f) Offset gather at iter. 20. (g) Raw gradient at iter. 10. (h) Approximated diagonal of Hessian at iter. 10. (i) Hessian corrected search direction.

fer to the numerator of equation (9) and the search direction is referred to $\widetilde{\delta c}$ which is the negative of the gradient corrected by the approximated diagonal of Hessian. In this example, the data is generated against a layered model as shown in fig.3(a). The starting velocity is homogeneous taking the value of top layer of the true velocity. Fig.3(b) shows the initial image. Three subsurface offset gathers are extracted from the left, middle and right of the model and is shown in fig.3(c) in left, middle and right, respectively. The corresponding inversion results at iteration 20 are shown in fig.3(d), fig.3(b) and fig.3(f) for velocity, image and subsurface gathers, respectively. It is interesting to note that as inversion proceeds the Hessian corrected search direction $\widetilde{\delta c}$ gradually moves to the deep. At iteration 10, the shallow velocity structures are fairly well reconstructed. Although the raw gradient (fig.3(g)) has energy concentrated at the shallow, the update $\widetilde{\delta c}$ is actually at the deep(fig.3(i)) after the correction from equation (9) by the approximated diagonal of Hessian(fig.3(h)).

The horizontal contraction in offset has a dual operation in angle, namely the horizontal dilation. When the image residual in offset is constructed with $-\partial_{|h|}I(x,h)$, the corresponding image residual in angle θ becomes $\partial_{|\theta|}I(x,\theta)$. Let Γ be the Radon transform from offset to angle, a residual in offset induced by angle dilation can be written as $R = \Gamma^*\partial_{|\theta|}\Gamma I$, where Γ^* (the transpose of Γ) approximates the inverse Radon transform Γ^{-1}. We report that the gradient that uses such R is also artifact-free in the presence of broken sub-horizontal reflectors.

3D FIELD DATA EXAMPLE

The 3d data consists of a few hundreds shots in three shot-lines with an end-on receiver geometry. Since the data contains too

few crosslines, we chose to construct only in-line sub-surface offsets. The initial velocity is taken as the vertical velocity from a joint VTI inversion of travel time tomography and FWI. For the isotropic migration this velocity is considered slower in total effect than that induced by the correct VTI velocity in VTI migration. The gradient using isotropic propagators from a hybrid image residual $R = (h^2 - \beta)I$ correctly captured this error. Shown in fig.4(a), the bulk color of the gradient is blue indicating the current velocity needs to be increased. Tracing vertically from the upper salt flank the gradient becomes oscillatory laterally. This is the typical gradient artifact introduced from many diffraction edges on the top salt. When the velocity model contains sharp edges usually introduced by truncations of faults, salts or complex geological structures, these gradient artifacts become dominant, particularly in the weak signal area. The velocity inversion therefore requires significant smoothing on gradients. Keeping everything else the same in equation (6) except changing the image residual to $-\partial_{|h|}I$, we obtain a gradient without edge effect which makes much more sense geologically even in the weak signal area.
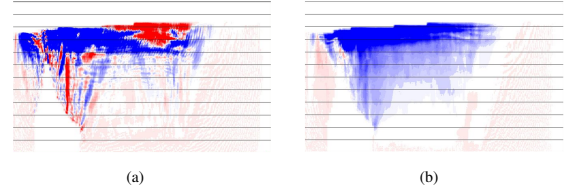

Figure 4: (a) Real data gradients from hybrid image residual $R = (h^2 - \beta)I$. (b) Real data gradient from image residual by radial derivative $R = -\partial_{|h|}I$.
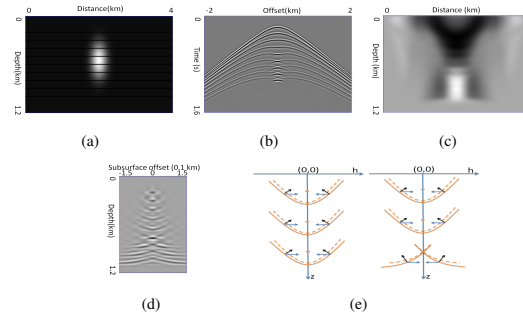
LENS EXAMPLE

Figure 5: (a) The true lens velocity and horizontal reflectors. (b) Shot gather directly above the lens. (c) The gradient obtained with constant velocity. (d) The offset gather in the middle of the model. (e) Schematic plot of image in offset for layered media (left) and for strong low velocity lens (right).

We report a lens example in which horizontal contraction produces a gradient that has sign errors. We generate Born data against 9 horizontal singular reflectors embedded in a 2D velocity model consists of a background velocity at 2000m/s and

a low lens centered with 1600m/s (fig.5(a)). The shot gather directly above the lens shows clear triplication (fig.5(b)). The gradient obtained with constant velocity at 2000m/s presents a sign flip on the bottom half in the model space. The Hessian correction only modifies the amplitude but keeps the sign unchanged. Lens data with different refracting strength repeat the same gradient pattern as shown in fig.5(c). We extract the very offset gather through the middle of the model. In fig.5(d) the offset runs from -150m to +150m horizontally. Shown in fig.5(e)(right) is a plot schematically represent the offset gather in fig.5(d). The data records the multivaluedness of traveltimes that manifests itself as a set of crossing events near zero subsurface offset. This is a phenomenon quite different from the layered case as demonstrated in fig.5(e)(left). We hypothesize that the correct total warping in order to produce an infinitesimally improved image is a perturbation towards the direction that increases the image curvature while keeping the image gather centered at zero offset. We see in the layered case, the direction of warping by horizontal contraction (blue arrow) form a less-than-$90°$ angle with the direction of total warping (black arrow). For the case of low lens velocities, this angle is bigger than $90°$ for deeper images where the multivaluedness break the horizontal smoothness of image at zero offset. In other words, the horizontal contraction is not a good approximation of the total warping if it cannot increase the resulting image curvature.

DISCUSSION

The essential contention of this paper is expressed in equation (5): a rule for constructing an image residual δI gives rise to a rule for a velocity update δc via least squares projection from image space to velocity space. An image residual is really a direction vector in image space: that is, for each image, an increment moving it closer to focus. Such an assignment of a direction to each point in a space amounts to a differential equation in the space, which in turn gives rise to an evolution flow. Table 1 describes the image evolution flow induced by several image residual constructions. The first two columns describe gradient flows induced by two versions of differential semblance, as described by Symes (2008). That is, the differential semblance image residual is itself the gradient of an objective function. The last column describes the horizontal contraction residual: it is not the gradient of an objective function.

All three flows have the same asymptotic limit sets, that is, focused images, and that is why all three generate constructive velocity updates via least squares projection (equation (5)), in some circumstances. The surface offset (or other acquisition parameter) differential semblance image residual results in the heat equation in offset, whose trajectories limit to images constant in offset, which is the focusing criterion for this type of image space. The related velocity update fails in the presence of multi-pathing, whereas the velocity updates generated by the differential semblance image residual in horizontal subsurface offset (column 2) remain constructive in strongly refractive velocity models so long the relevant rays do not turn horizontal (Symes, 2008). The flows for both the differential sem-

blance and $|h|$ scaled horizontal contraction (column 3) image residuals limit to images focused at zero offset, but in different ways: the differential semblance flow (column 2) simply "forgets" the initial image energy at nonzero offset, whereas the horizontal contraction flow incorporates it into the zero offset limit. This difference may be related to the presence, vs. absence, of artifacts described earlier in the velocity updates derived from differential semblance, respectively horizontal contraction, for sub-horizontal broken reflectors. On the other hand, differential semblance has performed well for velocity lens examples (Shen and Symes, 2008), whereas our examples above reveal that horizontal contraction apparently leads to velocity updates of the wrong sign.

Table 1: Evolution Induced by Residuals

	surface offset DS algorithm	subsurface offset DS algorithm	subsurface horizontal contraction
image residual	$-\partial_h^2 I$	$p^2(h)I$	$-|h|\partial_{|h|}I$
image evolution	$\frac{\partial I}{\partial t} = \partial_h^2 I$	$\frac{\partial I}{\partial t} = -p^2(h)I$	$\frac{\partial I}{\partial t} = |h|\partial_{|h|}I$
solution	constant at $t \to \infty$	$I = e^{-p^2(h)t}I_0$	$I = I_0(e^t h)$

CONCLUSION

We have shown that several recently suggested velocity update formulae, including variants of differential semblance, may be cast in the form of the least-squares projection into velocity space of an image residual (equation (5)). We have also shown how to implement the unit horizontal contraction velocity update efficiently, and given a first 3D example. Our work gives a dynamical systems interpretation to the update suggested by Fei and Williamson (2010), and verifies that horizontal contraction image residuals lead to smoother velocity updates and faster convergence, in comparison to "classical" differential semblance. Many image residuals besides differential semblance and horizontal contraction define flows that limit to focused images, hence potentially generate useful velocity updates. Most of these possibilities remain to be explored.

ACKNOWLEDGMENT

REFERENCES

Albertin, U., 2011, An improved gradient computationa for adjoint wave-equation reflection tomography: Expanded Abstracts, Society of Exploration Geophysicists, 81th Annual International Meeting, 3969–3973.

Fei, W. and P. Williamson, 2010, On the gradient artifacts in migration velocity analysis based on differential semblance optimization: Expanded Abstracts, Society of Exploration Geophysicists, 80th Annual International Meeting, 4071–4076.

Pratt, R. G., C. Shin, and G. J. Hicks, 1998, gauss-newton and full newton methods in frequency domain seismic waveform inversion: Geophysical Journal International, **133**, 341–362.

Sava, P., 2000, Prestack stolt residual migration for migration velocity analysis: Expanded Abstracts, Society of Exploration Geophysicists,70nd Annual International Meeting, 992–995.

Shen, P., 2012, An rtm based automatic migration velocity analysis in image domain: 82nd Ann. Internat Mtg., Soc. of Expl. Geophys.

Shen, P. and W. W. Symes, 2008, Automatic velocity analysis via shot profile migration: Geophysics, **73**, VE49–VE59.

Symes, W. W., 2008, Migration velocity analysis and waveform inversion: Geophysical Prospecting, **56**, 765–790.

Tarantola, A. and B. Vallette, 1982, Inverse problems: quest for information: J. Geophysics, **50**, 159–170.